Acta Cryst. (1995). A51, 143–153

Topological Definition of Crystal Structure: Determination of the Bonded Interactions in Solid Molecular Chlorine

BY V. G. TSIRELSON

Mendeleev University of Chemical Technology, Moscow 125047, *Russia*

AND P. F. ZOU,* T.-H. TANG AND R. F. W. BADER

Department of Chemistry, McMaster University, Hamilton, Ontario L8S 4M1, Canada

(*Received* 18 *May* 1994; *accepted* 15 *August* 1994)

Abstract

The heavier halide molecules form layered crystals indicative of the presence of a specific directed intermolecular interaction. It is shown that this interaction within the crystal can be defined and characterized using the topology of the electron density within the theory of atoms in crystals. It is also shown that its presence in the crystal and the resulting geometry of the layered structure can be predicted in terms of the topology of the Laplacian distribution of an isolated Cl_2 molecule, as it relates to the definition of Lewis acid and base sites within the valence shell of an atom. The generality of the definition of both primary and secondary interactions in terms of the topology of the electron density is demonstrated for all types of crystal. The electron density of solid molecular chlorine was determined by fitting the experimental X-ray structure factors and by theoretical calculation and its topology determined. Each Cl atom is found to be linked by bond paths, lines of maximum electron density, to twelve other atoms in the crystal: to four atoms in the same layer parallel to the *bc* plane, one of which defines the intramolecular bond of the Cl_2 group, to six atoms in the four neighbouring molecules lying in the same stack parallel to the *b* axis and to two atoms in molecules situated in a neighbouring stack.

Introduction

The crystal structures of the heavier halogens Cl_2, Br_2 and I_2 are layered, with all the atoms in the planes parallel to (100) (Fig. 1). This is not the structure anticipated for a crystal in which the intermolecular interactions may be described in terms of a non-directional van der Waals-type potential (Williams & Hsu, 1985). It is the purpose of this paper to demonstrate the presence of a short-contact intermolecular bond in terms of the distribution of both the measured and the calculated electron density of crystalline chlorine, and to show that the presence and directional property of this interaction can be predicted in terms of the charge distribution of the isolated molecule.

The van der Waals potential used in the description of a solid is assumed to be pairwise additive over the 'non-bonded' atoms and to consist of an attractive dispersion term and a repulsive exponential contribution. It is possible to assign a transferable non-bonded potential-energy function for each type of atom to predict the structures of so-called van der Waals crystals (Cox, Hsu & Williams, 1981; Williams & Cox, 1984; Williams & Weller, 1983). Such a function for a Cl atom, for example, satisfactorily describes the structures of crystalline perchlorohydrocarbons but fails when applied to solid chlorine (Hsu & Williams, 1979). When applied to the crystalline halogens, the model incorrectly predicts a nonplanar molecular packing which maximizes the number of 'non-bonded' interactions and the stabilizing contribution from the dispersion energy.

The failure of the van der Waals model to describe the halogen structures is not remedied by the inclusion of

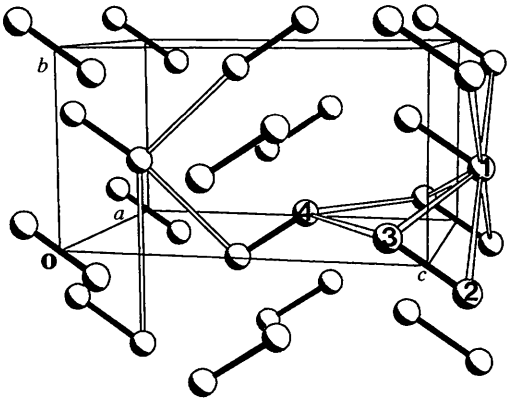

Fig. 1. The crystal structure of molecular chlorine. The solid lines denote the intramolecular bond paths defining the Cl_2 groups. The open lines denote the bond paths defining the secondary interactions, as discussed in the paper.

* Present address: Department of Chemistry, University of Toronto, Toronto, Ontario M5S 1A1, Canada.

quadrupole–quadrupole interactions (Yamasaki, 1962). Instead, the in-plane alignment of the molecules, which in the case of solid chlorine yields a nearest-neighbour contact of 3.28 Å, a value significantly less than twice the accepted van der Waals radius of 1.80 Å, was taken to indicate the presence of a specific intermolecular bond for the short contact, one that is characterized by a directional property that may not be described in terms of the isotropic van der Waals potential. Experimental evidence for such bonding in the heavy halogens, including lowering in the Raman stretching frequencies compared with the isolated monomers and an asymmetry in the electric field gradient at a Cl nucleus determined in nuclear quadrupole resonance measurements, have been reviewed by Williams & Hsu (1985). These authors supplemented the transferable Cl–Cl potential function with a single specific intermolecular bonding force constant for the short contact and obtained a satisfactory description of the crystal structure of molecular chlorine. However, as these authors point out, one can introduce anisotropy into the empirical model by modifying either the attractive or the repulsive contribution to the potential and agreement of a given model with an observed structure does not necessarily justify the assumptions made in the model.

Nyburg & Wong-Ng (1979), in criticizing an earlier model of solid Cl_2 (Hsu & Williams, 1979), proposed one that assumed that the non-bonded radius of a bound Cl atom is anisotropic, equivalent to a 'polar flattening' (Nyburg, 1979). In this manner, directional effects were introduced into the model potential between 'non-bonded atoms', a procedure involving a relatively large number of adjustable parameters. Nyburg (1979) assumed the flattening to be determined by the 'shape of the electron-density profile' of the free molecule and by a polarization of the bond as caused by the interaction. The use of isovalued envelopes of the electron density to assign a size and shape to a molecule involved in van der Waals or 'non-bonded' interactions was introduced and documented in 1967 (Bader, Henneker & Cade, 1967), attention being drawn to the very asymmetry in the non-bonded radius assumed by Nyburg (1979). Molecular shapes determined in this manner have been used to determine the packing of the α phase of O_2 (Barrett & Meyer, 1967; Barrett, Meyer & Wassermann, 1967) and of a number of solid phases of N_2, including those under high pressure (Mills & Schuch, 1969; Schuch & Mills, 1970; Raich & Mills, 1971; Schiferl, Cromer, Schwalbe & Mills, 1983).

These examples and other more recent work (Bader, Carroll, Cheeseman & Chang, 1987) demonstrate that the density envelopes, 0.001 a.u. for gases and 0.002 a.u. for solids, provide reliable measures of the molecular sizes and shapes determined by weak van der Waals interactions between closed-shell systems. This is not the case for solid chlorine. The halogens exhibit an anisotropic non-bonded shape (Bader, Henneker & Cade, 1967) as typified by the electron density of a Cl atom (Fig. 2), which possesses an axial non-bonded radius of 1.70 Å compared with a perpendicular radius of 1.92 Å (for the 0.002 a.u. envelope), their average equalling the accepted van der Waals radius of 1.8 Å. Thus, the short contact of 3.28 Å found in solid Cl_2 is a result of a significant penetration of the van der Waals envelopes of both the acid and base atoms. Such penetrations indicate the presence of a significant bonded interaction between closed-shell systems, the magnitude of the penetration paralleling the strength of the interaction, as documented in hydrogen-bonded systems, for example (Carroll & Bader, 1988). The Cl atom of HCl is penetrated by 0.39 Å when hydrogen-bonded to HF, compared with a penetration of 0.35 Å found here for the base Cl atom in the Cl_2 dimer, using the 0.001 a.u. envelope for gas-phase molecules.

One can appeal to the topology of the electron density $\rho(\mathbf{r})$ to obtain direct physical evidence of bonded interactions between specific pairs of atoms in any environment (Bader, Nguyen-Dang & Tal, 1979; Bader, 1990) including a crystal (Zou & Bader, 1994) and this is the procedure followed here. In addition, the density $\rho(\mathbf{r})$ and its Laplacian $\nabla^2\rho(\mathbf{r})$ provide a characterization of the interactions and an understanding of their presence in a crystal.

The electron-density distributions and the optimized geometries for the Cl_2 monomer and dimer were determined using *GAUSSIAN*92 (Frisch *et al.*, 1992) in a Møller–Plesset second-order perturbation (MP2) calculation using the 6-311^{++}G(2d) basis set. The *PROAIM* series of programs was used in the analysis of the theoretically determined density (Biegler-König, Bader & Tang, 1982). The electron density for solid chlorine was calculated using the program *CRYSTAL*, a Hartree–Fock procedure for extended systems (Pisani, Dovesi & Roetti, 1988). The 6-21G* basis set (Binkley, Pople & Hehre, 1980; Pisani, Dovesi & Orlando, 1992) was used and the calculation was performed for the unit-cell parameters obtained by Stevens (1979),† using the correct value for c. An experimental quasistatic electron density of solid chlorine was also determined using Stevens (1979) X-ray scattering data.

Determination of the bonded interactions in molecular crystals

Definition of a bond path and molecular structure

The theory of atoms in molecules defines an atom as a proper open system, one whose properties are predicted

† This paper contains a typographical error that is repeated by Williams & Hsu (1985), the value of the cell parameter c being incorrectly given as 8.117 Å instead of 8.177 Å. The incorrect value of c yields a Cl–Cl bond length of 1.981 Å, as opposed to the value of 1.991 Å quoted in the paper and a nearest-neighbour distance of 3.27 Å used by Williams & Hsu (1985), rather than the correct value of 3.28 Å.

by quantum mechanics (Bader, 1990, 1994). The condition defining the atom is stated in terms of the gradient vector field of the electron density $\rho(\mathbf{r})$. Atom Ω is defined as a region of real space bounded by a set of interatomic surfaces $S(\Omega, \Omega'; \mathbf{r})$, there being one such surface for each neighbouring atom Ω'. Each surface is unique as it exhibits a local zero flux in the field $\nabla\rho(\mathbf{r})$,

$$\nabla\rho(\mathbf{r}) \cdot \mathbf{n}(\mathbf{r}) = 0 \qquad (1)$$

for all points in $\mathbf{S}(\Omega, \Omega'; \mathbf{r})$ and for all neighbouring atoms. Atoms Ω and Ω' are neighbouring if there exists a critical point between them, a point where $\nabla\rho = 0$, at which one curvature of ρ is positive and two are negative, a (3,−1) critical point. The interatomic surface is defined by the set of trajectories of $\nabla\rho$ that *terminate* at the critical point, as illustrated for the Cl_2 dimer in Fig. 2. It is seen that the definition of an atom given in (1) is equivalent to defining it as the region of space (the atomic basin) traversed by all of the trajectories of $\nabla\rho$ that terminate at the nucleus of the atom. The same definition applies to a crystal where it can be used to generalize the definition of a Wigner–Seitz cell (Zou & Bader, 1994).

A unique pair of trajectories also *originate* at a (3,−1) critical point and terminate at each of the neighbouring nuclei (Fig. 2). They define a line through space linking the nuclei, along which the electron density is a maximum with respect to any neighbouring line, *an atomic interaction line*. The necessary but in general not sufficient condition for two atoms to be bonded to one another is that their nuclei be linked by an atomic interaction line (Bader, 1990). The presence of such a line indicates that electronic charge has been accumulated between the nuclei along the length of the line. This accumulation of electron density is a necessary condition for bonding because, if two nuclei are to be bound, not only must the (Hellmann–Feynman) forces acting on them vanish for some $R = R_e$, but there must in addition be net forces of attraction drawing the nuclei together over a range of internuclear separations $R > R_e$. This

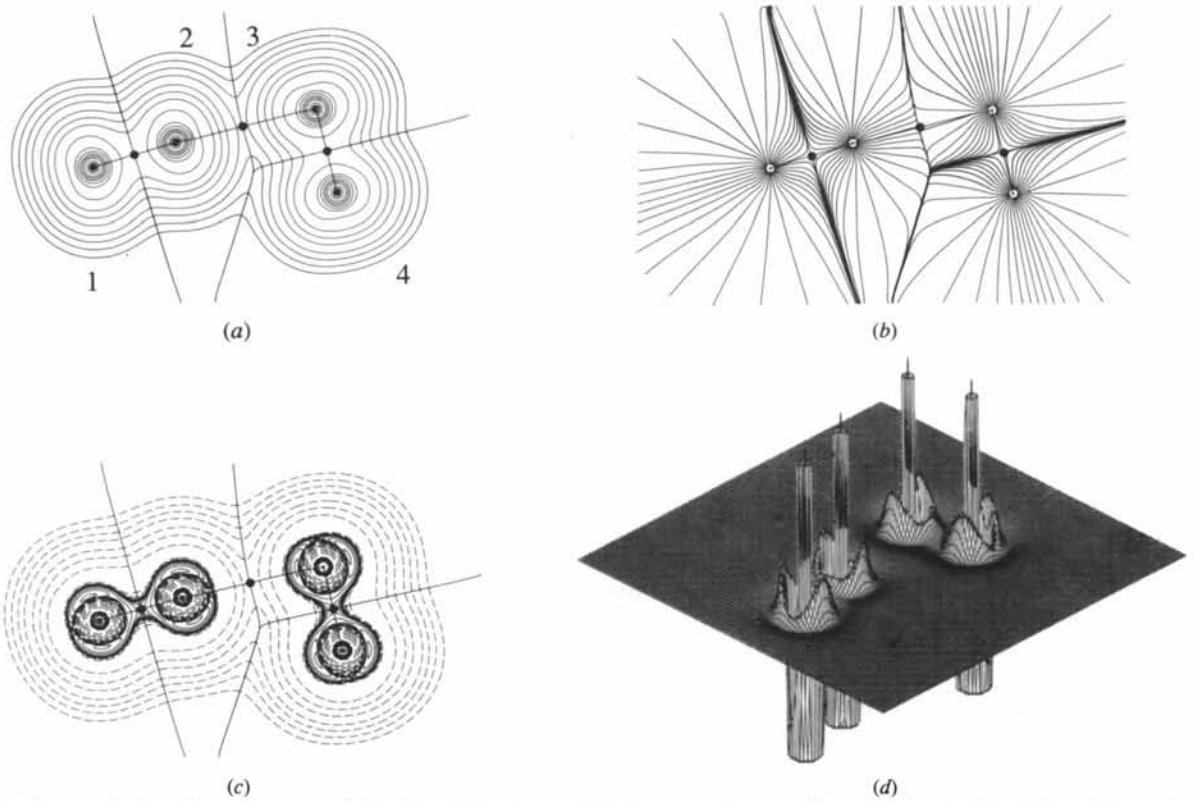

Fig. 2. (*a*) Electron density, (*b*) gradient vector field, (*c*) Laplacian (where dashed contours denote positive values) and (*d*) Laplacian relief map for the Cl_2 dimer. Each nucleus in (*b*), denoted by an open circle, serves as the terminus for the trajectories of $\nabla\rho$ that traverse its basin. The positions of the bond critical points are denoted by dots. The trajectories of $\nabla\rho$ that terminate at each dot and define the intersection of the interatomic surface with this plane are superimposed on maps (*a*) and (*c*), as are the bond paths. The Laplacian relief map (*d*) illustrates the three shells of charge concentration and the presence of the non-bonded charge concentrations and charge depletions (CCs and CDs, respectively) in the VSCCs of the Cl atoms. The geometry of the intermolecular interaction is determined by the alignment of a CD on one Cl with a CC on another. The outer contour for ρ is 0.001 a.u. and the remaining ones are in the order 2×10^n, 4×10^n and 8×10^n, with n beginning at −3 and increasing in steps of unity. The same set of contours is used in the following diagrams, with the label 1 denoting the contour of lowest value, 0.001 a.u. The same contour values are used in the Laplacian maps, the solid lines denoting negative values.

follows because it is the integral of the Hellmann–Feynman force on the nuclei over the same range of internuclear separations that determines the change in energy and only if the forces are attractive, as caused by the accumulation of density between the nuclei, will the energy decrease on the approach of the atoms.

The presence of an atomic interaction line in an equilibrium geometry indicates that sufficient electron density has indeed been accumulated to cause the forces on the nuclei to vanish and to yield a bound state. In this case, the presence of the interaction line is also a sufficient condition for the atoms to be bonded to one another and the line is then referred to as a bond path. A bond path is stable to the motions of the nuclei over the region of the potential energy surface where the system is bound.

A molecular graph is defined as the network of bond paths or atomic interaction lines linking the neighbouring nuclei. A molecular graph isolates the pairwise interactions present in an assembly of atoms that dominate and characterize its properties. It defines the system's molecular structure (Bader, Nguyen-Dang & Tal, 1979). The network of bond paths is found to coincide with the network of bonds generated by linking together those atoms that are assumed to be bonded to one another on the basis of chemical considerations. This has been illustrated for a multitude of systems, including those that lie beyond the electron-pair model of the chemical bond. The examples include acylic, cyclic and bicyclic hydrocarbons, both strained and unstrained (Wiberg, Bader & Lau, 1987), non-classical ions (Cremer *et al.*, 1983; Bader & Laidig, 1992), boranes and carbaboranes (Bader & Legare, 1992; Cioslowski & McKee, 1992), peptides (Chang & Bader, 1992; Popelier & Bader, 1994), hydrogen-bonded interactions and weak bonds (Cioslowski, Mixon & Edwards, 1991; Cioslowski & Mixon, 1992), metal–ligand complexes (Low, Kunze, MacDougall & Hall 1991; MacDougall & Hall, 1990) and materials in the solid state, including metals and alloys, semiconductors and insulators (Eberhart, Donovan, MacLaren & Clougherty, 1991; Eberhart, Clougherty & MacLaren, 1993; Eberhart, Donovan & Outlaw, 1992; Downs & Swope, 1992; Mei, Edgecombe, Smith & Heilingbrunner, 1993; Zou & Bader, 1994). A survey of applications is given by Bader (1991).

The topological definition of molecular structure is universal: a bond path can be associated with all types of interatomic interactions, including hydrogen-bonded and van der Waals interactions in theoretically determined densities (Carroll & Bader, 1988; Popelier & Bader, 1992) and in those determined experimentally (Kapphahn, Tsirelson & Ozerov, 1988; Stewart, 1991; Destro, Bianchi, Gatti & Merati, 1991). Thus, even van der Waals interactions that are modelled by 'non-bonded' isotropic potential functions generate intermolecular lines of maximum electron density that link particular nuclei and define an intermolecular structure for the crystal (Bader, 1990; Bone & Bader, 1995). The identification of a specific intermolecular interaction present in a system of molecules is illustrated in Fig. 2 by the bond path connecting the chlorine monomers in the dimer to yield a predicted intermolecular separation of 3.37 Å in an MP2 calculation (Table 1). Its presence in the electron-density distribution of solid chlorine and its identification with the short 3.28 Å contact in the crystal will be demonstrated below. The measured electron density can thus be used to identify the secondary interactions in molecular crystals and also in ionic solids. Fig. 3 illustrates the gradient vector field for the LiF crystal in (*a*) and for solid carbon dioxide in (*b*). In addition to the bond paths linking each Li atom to six neighbouring fluoride ions and the intramolecular bonds in carbon dioxide, 'secondary' interactions are defined in both crystals: a bond path linking O nuclei of two CO_2 molecules and a set of bond paths linking the next-nearest neighbouring F nuclei in the ionic crystal. Just as the network of bond paths defines the molecular structure

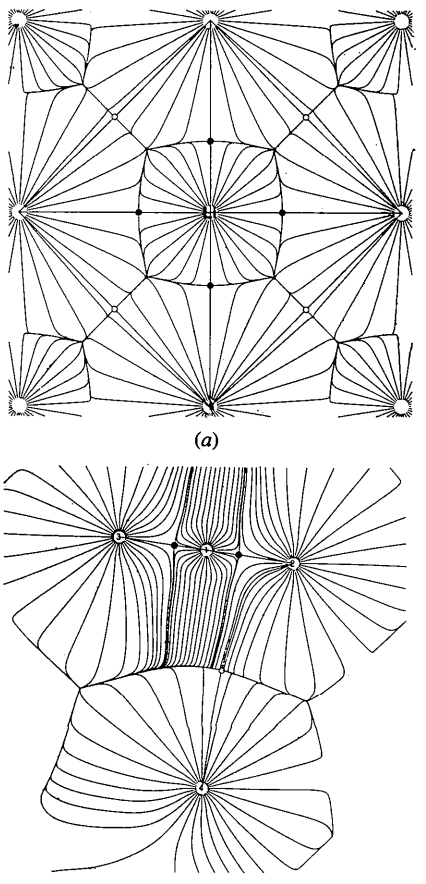

(*a*)

(*b*)

Fig. 3. The gradient vector fields for (*a*) an LiF crystal, Li is the central atom, and (*b*) solid carbon dioxide, nucleus 1 is carbon, 2, 3 and 4 are oxygen nuclei. The nearest-neighbour critical points are denoted by dots, those for the next-nearest neighbours by small open circles in these and the remaining figures.

Table 1. *Properties for* Cl_2 *dimer determined in an MP2//6-311*$^{++}$G(2d) *calculation*

Energy of dimer = −1838.590314 a.u., energy of monomer = −919.2938742 a.u. (R = 2.0263 Å).

Bond	Length (Å)	ρ_b (a.u.)	$\nabla^2\rho_b$ (a.u.)	$r_b(\Omega)$ (Å)	∠1–2–3†	∠2–3–4
Cl1–Cl2	2.0278	0.1493	−0.0596	1.016		
Cl3–Cl4	2.0278	0.1494	−0.0606	1.012		
Cl2–Cl3	3.3682	0.0067	+0.0296	1.774, 1.594‡	176.4°	90.40°

† See Fig. 2 for numbering of atoms.

‡ First value is the distance from critical point to nucleus of base atom, followed by the value for the acid atom. Corresponding non-bonded radii in monomer to 0.002 a.u. density envelope are 1.92 and 1.70 Å, respectively.

in an isolated molecule, it defines the crystal structure in a solid (Zou & Bader, 1994).

Characterization of atomic interactions

In addition to defining the structure present in any assembly of atoms, the electron density provides one with a characterization of the interactions so defined in terms of the quantities ρ_b and $\nabla^2\rho_b$, the values of the electron density and its Laplacian at the bond critical point. The value of ρ_b provides a measure of bond order for a series of bonds between similar atoms. For example, the ρ_b values for the C–C bonds in ethane, benzene, ethylene and acetylene yield bond orders of 1.0, 1.6, 2.0 and 3.0, respectively (Bader, 1990).

The Laplacian of a scalar field such as $\rho(\mathbf{r})$ determines where the field is locally concentrated $\nabla^2\rho < 0$ and locally depleted, $\nabla^2\rho > 0$. The topology is given in terms of $-\nabla^2\rho(\mathbf{r})$, a maximum in this function denoting a local concentration of electronic charge at $\mathbf{r}$. The electron density is a maximum in an interatomic surface at the bond critical point and the two associated curvatures of ρ, those perpendicular to the bond path, are therefore negative. Thus, electronic charge is concentrated in the surface at this point. The electron density is a minimum at this same point along the bond path, the third curvature of ρ being positive. Electron density is, therefore, locally depleted at the critical point with respect to neighbouring points along the bond path. Thus, the formation of an interatomic surface and chemical bond is a result of a competition between the perpendicular contractions of ρ, which lead to a concentration of electronic charge along the bond path, and the parallel expanion of ρ, which leads to its depletion in the surface and to its separate concentration in the basins of the neighbouring atoms. The sign of $\nabla^2\rho_b$ determines which of these two competing effects is dominant. The Laplacian of ρ appears in the local expression of the virial theorem, wherein it is related to the potential and kinetic energy densities (Bader, 1990). This theorem demonstrates that the lowering of the potential energy dominates the total energy in those regions of space where electronic charge is concentrated, where $\nabla^2\rho < 0$.

When $\nabla^2\rho_b < 0$, the perpendicular contractions of ρ dominate the interaction and electronic charge is concentrated between the nuclei along the bond path. The result is a sharing of electronic charge by both atoms, as found in bonds described as covalent and exemplified in Figs. 2(*c*) and (*d*) by the bond in a Cl_2 monomer group. Table 1 lists values of ρ_b and $\nabla^2\rho_b$. This concentration of charge results in a relatively large value of ρ_b and thus in a shared interaction, electron density is both accumulated and concentrated along the bond path between the nuclei. These interactions achieve their stability through the lowering of the potential energy resulting from the accumulation of electronic charge between the nuclei that is shared by both atoms.

The opposing extreme to a shared interaction occurs when two closed-shell systems interact, as found in ionic, hydrogen-bonded and van der Waals interactions. In such closed-shell interactions, the requirement of the Pauli exclusion principle leads to the removal of electron density from the region of contact, the interatomic surface. Thus, the positive curvature of ρ along the bond path is dominant, $\nabla^2\rho_b > 0$, and the interaction is characterized by the contraction of the electron density away from the surface and by its separate concentration in each of the atomic basins, as found for the intermolecular interaction in the Cl_2 dimer (Table 1). In van der Waals and hydrogen-bonded interactions, the charge distributions of both molecules polarize so as to facilitate the mutal penetration of their van der Waals envelopes (Carroll & Bader, 1988) and the resulting value of ρ_b is very nearly equal to the sum of the values of $\rho(\mathbf{r})$ at each of the points of penetration in the unperturbed molecules. Thus, electron density is not accumulated and a closed-shell interaction is characterized by a relatively low value for ρ_b.

The extent of penetration can be determined by comparing the bonded radius of atom Ω, $r_b(\Omega)$, the distance of a bond critical point from its nucleus, with its van der Waals radius in the unperturbed molecule. The bonded radii and their associated penetrations for the van der Waals interaction in the Cl_1 dimer are unequal (Fig. 2 and Table 1), a result of the asymmetry of the non-bonded density of a Cl atom noted in the *Introduction*, the radius of the atom approaching end-on, identified below as the acid, exhibiting the smaller of the two radii. The acid and base molecules are penetrated by 0.11 and 0.15 Å, respectively, in forming the dimer and the corresponding values of $\rho(\mathbf{r})$, 0.0033 and 0.0036 a.u., sum to a value that differs by only 0.0002 a.u. from the value of ρ_b for the resulting intermolecular bond (Table 1).

Fig. 2(*d*) contrasts the concentration of charge in the internuclear region of a Cl_2 group, a shared interaction, with its depletion at the position of the critical point between the Cl_2 groups in the closed-shell interaction. Closed-shell interactions achieve their stability by the lowering of the potential energy associated with the separate concentration of electron density in each of the atomic basins. Small values for ρ_b in closed-shell interactions do not necessarily imply weak interactions. Thus, while the values of ρ_b for highly ionic interactions are small in value, the transfer of charge from one atomic basin to the other results in a strong interaction and one again finds the bond strength to parallel the values of ρ_b through a series of ionic molecules. Closed-shell interactions between identical neutral atoms, as found here, correspond to van der Waals interactions and, in general, are weak.*

Topology of the Laplacian and alignment of acid and base molecules

The Laplacian of the electron density recovers the shell structure of an atom by displaying a corresponding number of alternating shells of charge concentration and charge depletion. The uniform sphere of charge concentration present in the valence shell of a free atom is distorted upon chemical combination to form local maxima and minima, as illustrated by the relief map of $\nabla^2\rho_b(\mathbf{r})$ for the dimer in Fig. 2(*d*). The number and relative position of the local maxima in $-\nabla^2\rho$; in the valence-shell charge concentration (VSCC) coincide with the Lewis model of localized electron pairs (Bader, Gillespie & MacDougall, 1988; Bader, 1990). A local charge concentration is a Lewis base or nucleophile, while a local charge depletion is a Lewis acid or electrophile. A chemical reaction corresponds to the combination of a charge concentration (CC) in the VSCC of the base with a charge depletion (CD) in the VSCC of the acid, the reactivity paralleling the magnitude of the CC and the depth of the CD. The geometry of approach of the acid and base molecules is predicted through the alignment of their corresponding (3,−3) and (3,+1) critical points in $-\nabla^2\rho$;. This predictive property of the Laplacian has been illustrated in many different reactions (Bader, 1990; Bader, 1991), including those as diverse as the approach of methane to the oxygen of a metal oxide surface (Aray, Rodriguez, Murgich & Ruette, 1993) to the geometries of hydrogen-bonded complexes (Carroll, Chang & Bader, 1988).

The geometry of the chlorine dimer is predicted by the topology of the Laplacian distribution. The VSCC of a chlorine atom in Cl_2, in addition to a bonded CC, exhibits a non-bonded charge concentration which, because of the cylindrical symmetry, necessarily assumes the form of a torus encompassing the molecular axis. In addition, there is a CD on this axis on the non-bonded side of the atom. The short van der Waals bond of 3.37 Å that results in the formation of the dimer corresponds to the interaction of the nonbonded CC on the atom of one molecule with the CD on the atom of another. All this is made clear in Figs. 2(*c*) and (*d*). The predicted angle of approach of the two molecules, as determined by alignment of the CD on Cl_2 with the torus of charge concentration on Cl3 of the other molecule is 101° compared with the calculated Cl2–Cl3–Cl4 angle of 90°. This agreement is satisfactory, as the energy surface for the bending motion is found to be extremely shallow, the energy increasing by only 0.3 kJ mol^{-1} for a change in angle of 10° in the MP2 calculation. Only a calculation that includes electron correlation predicts a small binding energy for the dimer, equal to 6.7 kJ mol^{-1}. The intermolecular separation and the associated Cl1–Cl2–Cl3 angle (Table 1) are close to the values of 3.27 Å and 170.4° found for the corresponding parameters in the solid characterizing the short van der Waals contact.

The loss of cylindrical symmetry results in the condensation of the torus of charge concentration on a Cl atom into a set of local maxima or CCs. Thus, the VSCC of the atom serving as the base in the dimer exhibits four distinct CCs, or (3,−3) critical points in $-\nabla^2\rho$. They correspond to the presence of four valence-electron pairs in the Lewis model: there is one bonded CC and the torus yields three non-bonded CCs, one of which serves as the Lewis base, the other two being situated above and below the plane of the nuclei. The asymmetry of the non-bonded radius of a Cl atom is readily traced to the form of its Laplacian distribution: a torus of charge concentration encircling the axis and an axial charge depletion. The Laplacian of N in N_2 exhibits an axial charge concentration and its non-bonded radii, parallel and perpendicular to the internuclear axis, are equal [see Bader (1990) for a listing of atomic dimensions for free and bound atoms].

The electron density and the structure of solid Cl_2

Solid chlorine exhibits the space group *Cmca* (No. 64) with the molecular layers parallel to the *bc* plane (Collin, 1952; Donohue & Goodman, 1965; Stevens, 1979). Each

* The magnitude of $\nabla^2\rho_b$ for the intramolecular Cl–Cl bond is small, a result typical of shared interactions between electronegative atoms. For example, each of the central bonds between the increasingly electronegative atoms in the isoelectronic series of molecules H_3C–CH_3, H_2N–NH_2, HO–OH and F–F possesses a large value for ρ_b, the characteristic feature of a shared interaction, but the value of $\nabla^2\rho_b$ increases from −0.708 a.u. for the C–C bond in ethane to +0.154 a.u. for the bond in fluorine, a reflection of the increase in the positive curvature of ρ from 0.28 a.u. in the former to 2.10 a.u. in the latter. The electron density of an F atom is not only tightly bound but is physically localized within its atomic basin. Whether the value of $\nabla^2\rho_b$ is greater or less than zero can depend upon the basis set. The value of $\nabla^2\rho_b$ for F_2 is found to be negative, equal to −0.045 a.u., and $\rho_b = 0.386$ a.u. for a very large basis set containing *f* functions. What is important is the trend in values and the knowledge that a bond with a large ρ_b and a small magnitude $\nabla^2\rho_b$ is one in which density is accumulated and concentrated along the bond path with large negative curvatures but its final distribution is dominated by the stress parallel to the bond.

molecule possesses a crystallographic inversion centre and lies in a mirror plane perpendicular to the *a* axis.

Critical points and structure determined by the theoretical electron density

The electron density for the solid, calculated for the experimental lattice parameters (Stevens, 1979), together with its gradient vector field and its Laplacian distribution for a (100) plane containing Cl_2 groups, are shown in Fig. 4. The data for the bond critical points are given in Table 2. Each critical point is labelled by its Wyckoff letter as listed in *International Tables for Crystallography* (Hahn, 1983) for the space group *Cmca* to fix its location and frequency of occurrence within the unit cell. The values of ρ_b and $\nabla^2\rho_b$ for the intramolecular bond critical point, label *a*, are similar to the values obtained for the critical point of the Cl_2 group in the dimer. The values calculated for the dimer molecule with a geometry determined by the corresponding parameters in the crystal and using the same 6-21G* basis set as used in the crystal calculation are given in Table 2 in parentheses. The agreement between crystal and dimer values of ρ_b and $\nabla^2\rho_b$ improves with this use of a common basis set, indicating that the bond in the monomer is only slightly perturbed by the formation of the crystal. Only this critical point exhibits the characteristics of a shared interaction.

The remaining critical points define bond paths that link Cl_2 molecules to one another *via* closed-shell

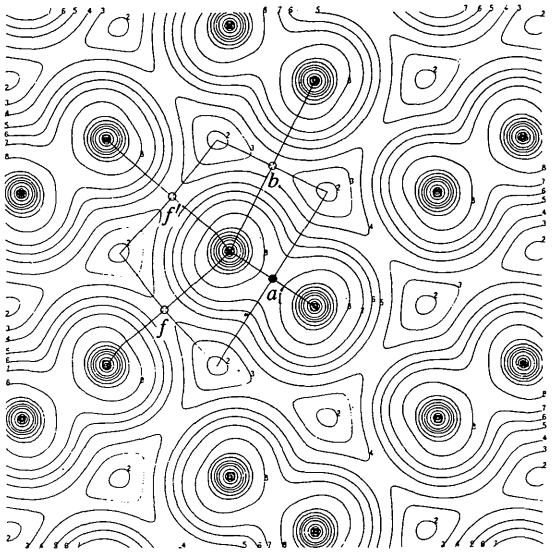

(*a*)

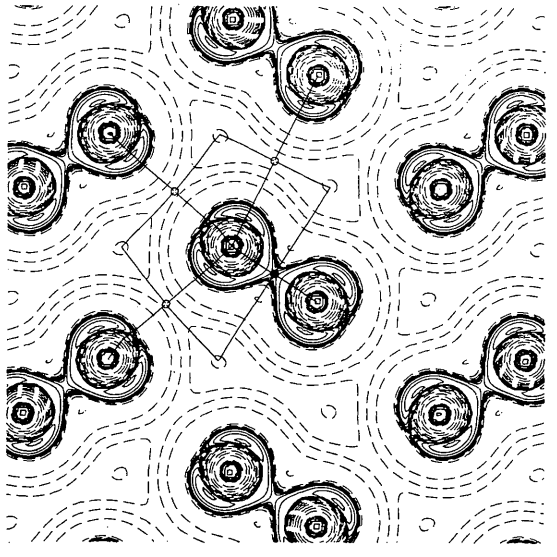

(*c*)

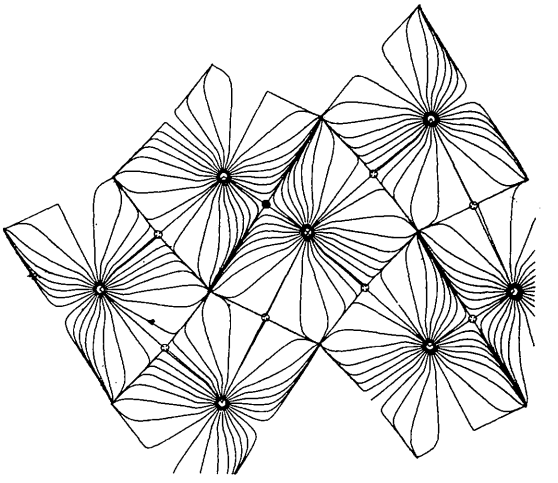

(*b*)

Fig. 4. The electron density, gradient vector field and Laplacian distribution for the (100) plane of solid chlorine, with solid contours denoting negative values for $\nabla^2\rho$, *i.e.* concentrations of charge. The bond paths and interatomic surfaces defined in the gradient map are illustrated for one atom superimposed on the density and its Laplacian. Three bond critical points are found in this plane: point *a* defining the intramolecular bond, points *f* and *f'* defining the 3.28 Å short contacts and point *b* the weaker in-plane interaction. The four bond paths linking one atom to other atoms in the same plane are illustrated in Fig. 1 for an atom in the left-hand stack of molecules.

Table 2. *Bond critical point data for solid chlorine*

Theoretical results calculated at experimental geometry with 6-21G* basis

Critical point multiplicity† and Wyckoff letter	ρ_b (a.u.)	$\nabla^2\rho_b$ (a.u.)	Length (Å)	r_b(Cl) (Å)
1 *a*	0.1546	−0.0595	1.991	0.996
	(0.1558)‡	(−0.0739)‡	1.991	0.996
2 *f*	0.00915	+0.0334	3.284	1.717 (base)
	(0.00918)‡	(+0.0331)‡	3.284	(1.717)‡
f'	0.00915	+0.0334	3.284	1.567 (acid)
1 *b*	0.00523	+0.0154	3.749	1.875
2 *c*	0.00531	+0.0172	3.703	1.851
4 *g*	0.00441	+0.0147	3.842	1.920
2 *e*	0.00331	+0.0106	3.938	1.969

Experimental results

Critical point and Wyckoff letter	ρ_b (a.u.)	$\nabla^2\rho_b$ (a.u.)	Length (Å)	r_b(Cl) (Å)
a	0.1460	+0.2863	1.991	0.996
f	0.0060	+0.0080	3.284	1.626 (base)
c	0.0068	+0.0162	3.697	1.848
e	0.0065	+0.0055	3.924	1.962

† Number of critical points per molecule.

‡ Values in parentheses are for an isolated dimer with a geometry to fit crystal parameters and using the same 6-21G* basis set used in the *CRYSTAL* calculation.

interactions, three of which, *f*, *f'* and *b* occur in the (100) plane. One notes that *f* and *f'*, symmetrically equivalent critical points for the bond path defining the short 3.28 Å contact responsible for the layered structure in the solid, exhibit all of the characteristics of the intermolecular bond path found in the dimer. As in the dimer, this bond path results from the interaction of the CD at the end of one molecule with a non-bonded CC on an atom of the neighbouring molecule (Fig. 4*c*). Each atom participates in two such interactions, serving as the Lewis base (*f*) in one and as the Lewis acid (*f'*) in the other. These bond paths exhibit the same kink in the neighbourhood of the acid-receptor hole as does the corresponding path in the isolated dimer. In addition to similar values for ρ_b and $\nabla^2\rho_b$ for dimer and crystal (see Table 1), the associated critical point is closer to the nucleus of the atom serving as the acid than to the one serving as the base, the bonded radii being identical in the dimer and crystal for the same basis set and geometry (Table 2). In terms of closeness of approach and value of ρ_b, the interaction labelled *f* is the strongest of the secondary interactions present in solid chlorine.

In addition to the bonding of a given atom to its nearest neighbour through a shared interaction, critical point *a*, and to its two next-nearest neighbours in closed-shell interactions, critical points *f* and *f'*, each atom is bonded to a fourth atom in the same (100) plane, as characterized by critical point *b*. Reference to Fig. 4(*c*) shows that the associated bond path, which represents a weaker interaction than that labelled *f*, results from the interaction of nonbonded CCs located on the two atoms. The formation of a bond path between two CCs can occur not only between two open-shell atoms to yield a shared interaction but also between two nonbonded CCs in a closed-shell secondary interaction when the nonbonded CCs are brought into juxtaposition by the primary bonds. The weakly bound CO_2 dimer is planar with one molecule displaced relative to the other so that a hole in the VSCC of the carbon in one O=C=O is opposed to a non-bonded CC in the VSCC of an O atom in the second O=C=O. The bond path, however, links the two non-bonded CCs on the pair of O atoms involved in the interaction (Bone & Bader, 1995). A transannular bond path linking non-bonded CCs of a pair of electron-rich sulfur atoms results when S_8^{2+} is formed from the neutral molecule and a pair of such bonds link two Cl_2^+ ions in Cl_4^{2+} to form a ring, the doubly charged ion serving as a model for I_4^{2+} in crystals of $I_4^{2+}.(AsF_6^-)_2$. In all of these examples, the value of ρ_b is relatively small, 0.04 a.u. or less, and $\nabla^2\rho_b > 0$, the characteristics of a weak closed-shell interaction. In general, a closed-shell interaction with a bond path linking a CD on the acid with a CC on the base, as found in the short secondary interaction in solid chlorine and in hydrogen-bonded complexes where a CC of an atom in the base interacts with an axial CD in the VSCC of the H atom, are stronger than those resulting from the interaction of two nonbonded CCs.

The intersection of the interatomic surfaces with the (100) plane associated with the four bond paths that link a single atom to its neighbours define the boundary of a Cl atom in this plane (Fig. 4). The point of intersection of a pair of such surfaces is a ring critical point, a (3,+1) critical point in the electron density, with $\rho = 1.76 \times (-3)$ and $\nabla^2\rho = 7.86 \times (-3)$ a.u.

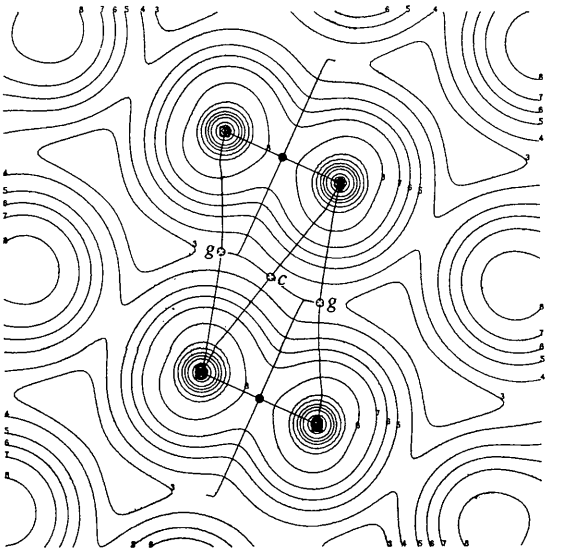

Fig. 5. Contour map of the electron density for a plane containing the critical points *c* and *g* that define the bond paths linking atoms within a given stack of molecules. The six bonds linking atom 1 in the right-hand stack to other atoms in the same stack are illustrated in Fig. 1.

The staggered chains of Cl molecules in neighbouring (100) layers are linked together by three different sets of secondary interactions, all defined by the gradient vector field of the electron density. Consider first the plane and bond paths illustrated in Fig. 5 which contains two of these, critical points *c* and *g*. This plane is obtained by translating one Cl_2 molecule into a second one lying half of a unit along the *a* axis and half of a unit along the *b* axis, as illustrated in Fig. 1. The critical point *g* characterizes the bond paths that link a given atom (labelled 1 in Figs. 1 and 5) to four others, two directly above it and two directly below, of four molecules lying in the same stack along the *b* axis. The shorter stronger interaction, characterized by critical point *c*, links the same atom to the second atom in just two of these molecules, as indicated in Fig. 1.

The plane containing point *e*, the final type of intermolecular bond critical point, is defined by the coordinates of the atoms labelled 2, 3 and 4 in Fig. 1. The critical point and its associated bond path as defined by the gradient vector field are illustrated in Fig. 6. Two such bond paths link a given atom in one layer with atoms of two other molecules in adjacent layers located in the neighbouring stack. These links between adjacent stacks of molecules are the longest and weakest of the intermolecular interactions.

Thus, a given Cl atom is linked by bond paths to 12 other atoms within the crystal. The strongest of these is the shared interaction *a* to give a Cl_2 group. This group, like the individual atom illustrated in Fig. 4, is a well defined unit, bounded by a set of zero-flux interatomic surfaces with a defined set of properties. The remaining interactions differ, not only in possessing longer bond-path lengths, but also represent the opposite extreme of binding, as characterized by their positive values of $\nabla^2\rho_b$ and smaller bond orders measured in terms of the values of ρ_b. The strongest of these interactions and the one that imparts the layered structure to the crystal results from the alignment of a non-bonded CC on one atom with the CD on another. Each atom participates in two of these interactions, as a base in one and as an acid in the other with other atoms in the same *bc* layer. There is another longer and weaker interaction with a third atom in this layer. Each atom is, in addition, bonded to six other atoms in molecules within the same stack and to two atoms in molecules in an adjacent stack. Thus, in terms of number and strength of the secondary interactions, the layering is the dominant structural feature with the stacking of molecules along axes parallel to the *b* axis next, followed by the interactions between the molecules in adjacent stacks. The interactions between adjacent stacks are both the fewest in number and the weakest. The identification of the bond critical points by their Wyckoff letter presented here is in agreement with their multiplicities listed by Hahn (1983) in the table for the space group *Cmca* (No. 64).

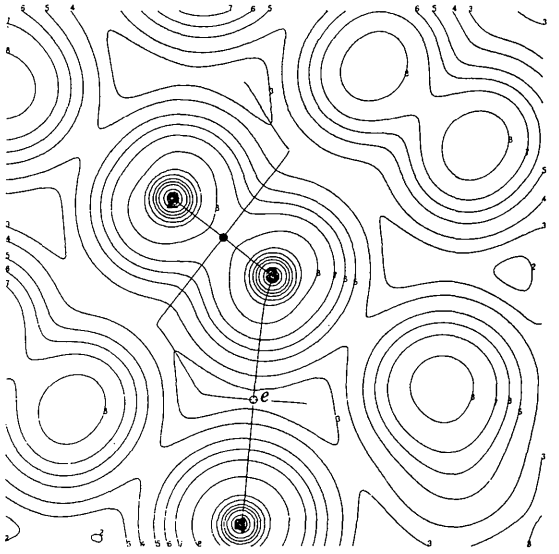

Fig. 6. Contour map of the electron density for a plane containing the critical point *e* that defines the bond path linking atoms in adjacent stacks of molecules. The bond paths linking atom 4 in the central stack to two others in a neighbouring stack are illustrated in Fig. 1.

Critical points and structure determined by the experimental electron density

Experimental electron-density deformation maps for solid chlorine were constructed by Stevens from his measured X-ray diffraction results obtained at 90 K (Stevens, 1979). The maps indicate the presence of two bonding peaks, each displaced 0.3 Å from the mid-point of the intermolecular bond, rather than an anticipated single bonding peak. Deformation maps defined relative to spherical-atom densities can fail to indicate the presence of bonding density between pairs of electronegative atoms (Dunitz & Seiler, 1983). The principal feature found by Stevens is a torus of density increase encircling the internuclear axis of a Cl_2 unit in the non-bonded region of each Cl atom at a distance 0.7 Å from the nucleus. Both the bonded and non-bonded features of the experimental maps are similar in appearance to the corresponding maxima exhibited by the theoretical Laplacian distributions for isolated and bound Cl molecules: each Cl atom exhibits a torus of non-bonded density peaking at 0.6 Å from the nucleus and a smaller bonded peak at 0.7 Å from the nucleus, the same distance found for the corresponding feature in the deformation map.

Stevens's (1979) data were used to obtain an experimental quasistatic electron density of solid chlorine using his cell parameters. The multipole model of Hansen & Coppens (1978) was used in the expansion for the electron density, refinement *F* in Table 5 of Stevens's work. By using a cluster of 14 pseudoatoms centred about a Cl molecule, the electron density of this molecule was found to be invariant to within 0.01% to

further cluster expansion. Thus, the final accuracy of the electron density is dependent upon the degree of success achieved during the structural model refinement and in the separation of the asphericity of the density of the pseudoatom from the anisotropy resulting from the anharmonic thermal motions. The topological properties were calculated analytically in position space.

The experimental density does indicate the presence of bond critical points (Table 2) and, unlike the deformation density, the total electron density does indicate the presence of intra- and intermolecular bonds within the crystal. In addition, the experimental Laplacian distribution exhibits a torus of non-bonded electron density centred on each Cl nucleus and encircling the internuclear axis of a Cl_2 unit. The map demonstrates, in agreement with the corresponding theoretical maps for the solid and the isolated dimer, that the short van der Waals interaction results from the alignment of the CD in the VSCC of one atom with the torus of charge concentration on another (Fig. 7).

The bond critical points found in the experimental electron density are listed in Table 2. Point *a* for the intramolecular bond and point *f* for the short contact van der Waals bond are among the critical points located in the crystal. There is fair agreement between the experimental and theoretical values of ρ_b and $\nabla^2\rho_b$, but the ordering of the strength of the secondary interactions is not the same. In addition, the experimental density yields a positive value of $\nabla^2\rho_b$ for the shared intramolecular interaction, a result associated with a lower-quality basis set in a theoretical calculation. The analyses of the experimental electron density and its Laplacian distribution do, however, substantiate the major features of the structure assigned to solid chlorine on the basis of the properties of the theoretical electron density.

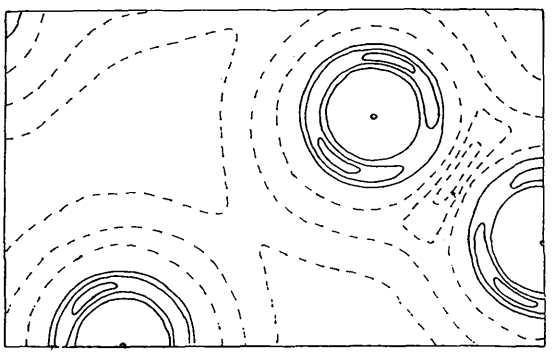

Fig. 7. Map of the Laplacian distribution for solid molecular chlorine (solid contours denote charge concentrations) calculated from the density expressed in terms of multipole density functions, as determined by a fit to the experimental structure factors (Stevens, 1979). This map recovers the essential feature of the short contact imparting the layered structure to the crystal, which is that it results from the interaction of a CD at the end of one molecule with a non-bonded CC on another.

Concluding remarks

The topology of the electron density coupled with the theory of atoms in molecules enables one to assign and characterize not only the primary interactions in a solid, *i.e.* intramolecular interactions in a molecular crystal and ion–cation interactions in an ionic crystal, but also the secondary interactions between molecules and between ions of similar charge. The presence of a bond critical point denotes the presence of a line of maximum electron density linking the neighbouring nuclei, as required for a stabilizing interaction between the atoms. The number and order of the interactions as monitored by ρ_b determine the relative stability of structural units within the crystal (*e.g.* layers of stacks) and thus the preferred cleavage planes.

The alignment of local charge concentrations with localized charge depletions, as defined by the topology of the Laplacian of the electron density, enables one to understand an observed crystal structure and to predict its possible form in terms of the properties of its isolated components.

The National Sciences and Engineering Research Council of Canada is thanked for an International Scientific Exchange Award enabling V. Tsirelson to visit McMaster University. We also wish to thank Professor P. Zorky, Dr A. Masunov and Dr S. Vyboischikov of Moscow State University for their collaboration in the calculation of the experimental Laplacian distribution.

References

ARAY, Y., RODRIGUEZ, J., MURGICH, J. & RUETTE, F. (1993). *J. Phys. Chem.* **97**, 8393–8398.
BADER, R. F. W. (1990). *Atoms in Molecules – a Quantum Theory*. Oxford Univ. Press.
BADER, R. F. W. (1991). *Chem. Rev.* **91**, 893–928.
BADER, R. F. W. (1994). *Phys. Rev. B*, **49**, 13348–13356.
BADER, R. F. W., CARROLL, M. T., CHEESEMAN, J. R. & CHANG, C. (1987). *J. Am. Chem. Soc.* **109**, 7968–7979.
BADER, R. F. W., GILLESPIE, R. J. & MACDOUGALL, P. J. (1988). *J. Am. Chem. Soc.* **110**, 7329–7336.
BADER, R. F. W., HENNEKER, W. H. & CADE, P. E. (1967). *J. Chem. Phys.* **46**, 3341–3363.
BADER, R. F. W. & LAIDIG, K. E. (1992). *J. Mol. Struct. (Theochem)*, **261**, 1–20.
BADER, R. F. W. & LEGARE, D. A. (1992). *Can. J. Chem.* **70**, 657–676.
BADER, R. F. W., NGUYEN-DANG, T. T. & TAL, Y. (1979). *J. Chem. Phys.* **70**, 4316–4329.
BARRETT, C. S. & MEYER, L. (1967). *Phys. Rev.* **160**, 694–697.
BARRETT, C. S., MEYER, L. & WASSERMAN, J. (1967). *J. Chem. Phys.* **47**, 592–597.
BIEGLER-KÖNIG, F. W., BADER, R. F. W. & TANG, T.-H. (1982). *J. Comput. Chem.* **13**, 317–328.
BINKLEY, J. S., POPLE, J. A. & HEHRE, W. J. (1980). *J. Am. Chem. Soc.* **102**, 939–947.
BONE, R. G. A. & BADER, R. F. W. (1995). In preparation.
CARROLL, M. T. & BADER, R. F. W. (1988). *Mol. Phys.* **65**, 695–722.
CARROLL, M. T., CHANG, C. & BADER, R. F. W. (1988). *Mol. Phys.* **63**, 387–405.

CHANG, C. & BADER, R. F. W. (1992). *J. Phys. Chem.* **96**, 1654–1662.
CIOSLOWSKI, J. & MCKEE, M. L. (1992). *J. Phys. Chem.* **96**, 9264–9268.
CIOSLOWSKI, J. & MIXON, S. T. (1992). *Can. J. Chem.* **70**, 443–449.
CIOSLOWSKI, J., MIXON, S. T. & EDWARDS, W. D. (1991). *J. Am. Chem. Soc.* **113**, 1083–1085.
COLLIN, R. L. (1952). *Acta Cryst.* **5**, 431–432; erratum (1956), **9**, 537.
COX, S. R., HSU, L. Y. & WILLIAMS, D. E. (1981). *Acta Cryst.* A**37**, 293–301.
CREMER, D., KRAKA, E., SLEE, T. S., BADER, R. F. W., LAU, C. D. H., NGUYEN-DANG, T. T. & MACDOUGALL, P. J. (1983). *J. Am. Chem. Soc.* **105**, 5069–5075.
DESTRO, R., BIANCHI, R., GATTI, C. & MERATI, F. (1991). *Chem. Phys. Lett.* **186**, 47–52.
DONOHUE, J. & GOODMAN, S. H. (1965). *Acta Cryst.* **18**, 568–569.
DOWNS, J. W. & SWOPE, R. J. (1992). *J. Phys. Chem.* **96**, 4834–4840.
DUNITZ, J. D. & SEILER, P. (1983). *J. Am. Chem. Soc.* **105**, 7056–7058.
EBERHART, M. E., CLOUGHERTY, D. P. & MACLAREN, J. M. (1993). *J. Mater. Res.* **8**, 438–448.
EBERHART, M. E., DONOVAN, M. M., MACLAREN, J. M. & CLOUGHERTY, D. P. (1991). *Prog. Surf. Sci.* **36**, 1–34.
EBERHART, M. E., DONOVAN, M. M. & OUTLAW, R. A. (1992). *Phys. Rev. B*, **46**, 12744–12747.
FRISCH, M. J., TRUCKS, G. W., HEAD-GORDON, M., GILL, P. M. W., WONG, M. W., FORESMAN, J. B., JOHNSON, B. G., SCHLEGEL, H. B., ROBB, M. A., REPLOGLE, E. S., GOMPERTS, R., ANDRES, J. L., RAGHAVACHARI, K., BINKLEY, J. S., GONZALEZ, C., MARTIN, R. L., FOX, D. J., DEFREES, D. J., BAKER, J., STEWART, J. J. P. & POPLE, J. A. (1992). Gaussian, Inc., Pittsburgh, PA, USA.
HAHN, T. (1983). *International Tables for Crystallography*, Vol. A. Boston: Kluwer Academic Publishers.
HANSEN, N. K. & COPPENS, P. (1978). *Acta Cryst.* A**34**, 909–921.
HSU, L. Y. & WILLIAMS, D. E. (1979). *Inorg. Chem.* **18**, 79–82.
KAPPHAHN, M., TSIRELSON, V. G. & OZEROV, R. P. (1988). *Port. Phys.* **19**, 213–216.
LOW, A. A., KUNZE, K. L., MACDOUGALL, P. J. & HALL, M. B. (1991). *Inorg. Chem.* **30**, 1079–1086.
MACDOUGALL, P. J. & HALL, M. B. (1990). *Trans. Am. Crystallogr. Assoc.* **26**, 105–123.
MEI, C., EDGECOMBE, K. E., SMITH, V. H. & HEILINGBRUNNER, A. (1993). *Int. J. Quantum Chem.* **48**, 287–293.
MILLS, R. L. & SCHUCH, A. F. (1969). *Phys. Rev. Lett.* **23**, 1154–1156.
NYBURG, S. C. (1979). *Acta Cryst.* A**35**, 641–645.
NYBURG, S. C. & WONG-NG, W. (1979). *Inorg. Chem.* **18**, 2790–2791.
PISANI, C., DOVESI, R. & ORLANDO, R. (1992). *Int. J. Quantum Chem.* **42**, 5–33.
PISANI, C., DOVESI, R. & ROETTI, C. (1988). *Hartree–Fock Ab Initio Treatment of Crystalline Systems, Lecture Notes in Chemistry*, Vol. 48. Heidelberg: Springer-Verlag.
POPELIER, P. L. A. & BADER, R. F. W. (1992). *Chem. Phys. Lett.* **189**, 542–548.
POPELIER, P. L. A. & BADER, R. F. W. (1994). *J. Phys. Chem.* **98**, 4473–4481.
RAICH, J. C. & MILLS, R. L. (1971). *J. Chem. Phys.* **55**, 1811–1817.
SCHIFERL, D., CROMER, D. T., SCHWALBE, L. A. & MILLS, R. L. (1983). *Acta Cryst.* B**39**, 153–157.
SCHUCH, A. F. & MILLS, R. F. (1970). *J. Chem. Phys.* **52**, 6000–6008.
STEVENS, E. D. (1979). *Mol. Phys.* **37**, 27–45.
STEWART, R. F. (1991). *The Application of Charge Density Research to Chemistry and Drug Design*, edited by G. A. JEFFREY & J. F. PINIELLA, pp. 63–102. NATO ASI Series B, No. 250.
WIBERG, K. B., BADER, R. F. W. & LAU, C. D. H. (1987). *J. Am. Chem. Soc.* **109**, 985–1000.
WILLIAMS, D. E. & COX, S. R. (1984). *Acta Cryst.* B**40**, 404–417.
WILLIAMS, D. E. & HSU, L.-Y. (1985). *Acta Cryst.* A**41**, 296–301.
WILLIAMS, D. E. & WELLER, R. R. (1983). *J. Am. Chem. Soc.* **105**, 4143–4148.
YAMASAKI, K. (1962). *J. Chem. Soc. Jpn*, **17**, 1262–1267.
ZOU, P. F. & BADER, R. F. W. (1994). *Acta Cryst.* A**50**, 714–725.

Acta Cryst. (1995). A**51**, 153–158

Simulation of Short-Range Order in F.C.C. Alloys

BY S. H. RAHMAN AND M. RODEWALD*

Institut für Mineralogie, Universität Hannover, Welfengarten 1, 30167 *Hannover, Germany*

(*Received* 22 *March* 1994; *accepted* 1 *August* 1994)

Abstract

The videographic simulation algorithm has been further developed to enable any distribution or vector correlation among atoms or structure variants beyond the first shell. The simulation method is applied to Ni_4Mo, Au_4Mn and Cu_3Au in order to describe their real structures above T_c. One of the main advantages of the method is the rapid calculation of the diffraction pattern from the simulated videographic structure image (parallel processing). Moreover, the 3D simulation field can be analysed to determine the local atomic arrangement or to calculate short-range-order parameters. The method can generally be applied to simulate defect or vacancy distributions with a specific degree of correlation.

Introduction

In order to characterize the local atomic arrangement of an alloy above the critical temperature (T_c), the Warren–Cowley short-range-order parameters a_{lmn} are used (Cowley, 1950).

To assist in the interpretation of the atomic configuration for the short-range-ordered state of alloys, Gehlen & Cohen (1965) conducted computer simulations based on experimentally measured short-range-order parameters (a_{lmn}). These Monte Carlo simulations were

* Present address: Fachbereich Materialwissenschaften, Fachgebiet Strukturforschung, Technische Hochschule Darmstadt, Petersenstrasse 20, 64287 Darmstadt, Germany.